

High resolution spectroscopy of H II Galaxies: Structure and Supersonic line widths

Eduardo Telles

Observatório Nacional, Rua José Cristino, 77, 20921-400 - Rio de Janeiro - BRASIL

etelles@on.br

Casiana Muñoz-Tuñón

Instituto de Astrofísica de Canarias, E-38200 La Laguna, Tenerife, SPAIN

cmt@ll.iac.es

and

Guillermo Tenorio-Tagle

INAOE, Apartado Postal 51, Puebla, Pue. MEXICO

gtt@inaoep.mx

ABSTRACT

We present high resolution echelle spectroscopy of a sample of H II galaxies. In all galaxies we identify different H α emitting knots along the slit crossing the nucleus. All of these have been isolated and separately analyzed through luminosity and size *vs* σ diagnosis plots. We find that in all cases, for a particular galaxy, the bulk of emission comes from their main knot and therefore, at least for the compact class galaxies, we are dealing with, luminosity and sigma values measured using single aperture observations would provide similar results to what is obtained with spatially resolved spectroscopy. In the size *vs* σ plots as expected there is a shift in the correlations depending on whether we are including all emission in a single point or we split it in its different emitting knots. The problem of a proper determination of the size of the emitting region so that it can be used to determine the mass of the system remains open. From the data set gathered, using the highest surface brightness points as recently proposed by Fuentes-Masip et al. (2000), the best luminosity *vs* σ correlation turns out to be consistent with a Virial model.

Subject headings: - galaxies: starburst – galaxies: structure – galaxies: line width

1. Introduction

H II galaxies are a subsample of dwarf galaxies with a strong star formation activity leading to intense nebular lines easy to detect in objective prism surveys. The optical properties of H II galaxies are dominated by their strong emission line spectra superposed on a weak blue continuum. The question, posed by Sargent & Searle (1970) of whether these are young galaxies forming stars for the first time seems now to have been

answered by recent studies. H II galaxies show an underlying stellar population of intermediate to old ages (Telles & Terlevich 1997, Doublier *et al.* 1997, Marlowe *et al.* 1999, Cairós *et al.* 2000). The optical/near-IR colors of their underlying galaxies are similar to late type dwarf galaxies, although their structural parameters derived from brightness profiles indicate that H II galaxies are more compact than late type quiescent dwarfs (Telles & Sampson 2000; Telles *et al.* 1999).

Their morphological classification splits them

into two groups: Type I includes the most luminous H II galaxies, all of which present an overall irregular morphology. Types II's, on the other hand, are more compact and rounder and present a luminosity profile similar to that of dwarf spheroidal galaxies (Telles, 1995). The few H II galaxies found to have a bright neighbor (maybe by chance) are all Type II's of regular morphology, contrary to what one would expect if galaxy interactions could be held responsible for the morphological disturbances found in Type I's (Telles & Terlevich 1995). In addition, H II galaxies as a class are not preferentially clustered around faint low mass galaxies (Telles & Maddox 2000), but some are found to have HI companions (Taylor 1997). The triggering mechanism of the present starburst in H II galaxies is not at all clear, yet for these dwarfs internal processes must play a major role.

Here we show echelle data obtained at the William Herschel telescope (4.2m) at the "Observatorio del Roque de los Muchachos" (ORM) at La Palma on a sample of type II dwarfs. Our high resolution echelle data show a strong variation in the line profiles across the emitting region and even in the most compact sources, there is an indication of separate knots of star formation (SF) evolving concurrently within the galaxy nucleus. The presence of multiple knots of star formation within the line emitting regions are also observed on high spatial resolution images, in particular in the near-IR. Telles *et al.* (1999, 2000) also identified knots which are possible super stellar clusters (SSC). Their individual properties may impose further constraints on the history of SF of a galaxy as well as indicate possible mechanisms able to trigger the present burst.

For our sample here we have defined different apertures across the H α luminosity profile and have extracted the spectra corresponding to different emitting knots in every object. Also the *total* spectra was obtained to mimic single aperture observations (Melnick *et al.* 1988), when it includes the ensemble of individual knots.

The structure found in H II galaxies has profound implications on several topics. In particular on issues such as star formation and its possible sequential propagation in H II galaxies, and how is the ISM structured in these galaxies. Another issue central in this field of research is the validity

of the interpretation, and use of the empirical correlations, of size and luminosity *vs* their supersonic line widths for high redshift galaxies. These correlations were first found for Giant H II Regions by Melnick (1979), Terlevich & Melnick (1981) and Melnick *et al.* (1987) and extended to H II galaxies by Melnick *et al.* (1988) and Telles & Terlevich (1993). The fact that Giant H II Regions and H II galaxies have supersonic motions and follow the same correlations have made us use and refer to the whole ensemble of objects as a single family. This may indicate that process of massive cluster formation is similar in both H II galaxies and Giant H II Regions and it is the main reason as to why we will not differentiate between them in discussing their dynamical properties. Here we describe in Section 2 and 3 our selected sample and observational strategy, and Section 4 presents full detail of the results for each galaxy. A general discussion and a summary of the results is given on Section 5.

2. The Observations

We have carried out long-slit echelle observations of a sample of 7 H II galaxies (see Table 1) with the Utrecht Echelle spectrograph at the 4.2-m William Herschel Telescope at the "Roque de los Muchachos" observatory, La Palma, Spain, on the nights of 30-31/05/1997. Exposures of 1200s were obtained using a 2148 \times 2148 Tek CCD and the 79.0 lines/mm echelle, reaching typical of S/N per pixel ≥ 30 at H α . The orders covered are 55 to 30, from $\sim 4130 \text{ \AA}$ - 7340 \AA , including H β and H α with short slit 19" mode (Mrk 36, UM 461, UM 533, Mrk 930) and order 34, from $\sim 6500 \text{ \AA}$ - 6650 \AA on H α with long slit 250 " mode (Mrk 59, II Zw 40, VII Zw 403). The spectral resolution (FWHM) of our setup was 0.13 \AA in the H β region and 0.18 \AA in the H α region. This led to a resolution of $\sim 8 \text{ km s}^{-1}$. The CCD frames were reduced using standard procedures with the tasks in IRAF. The data was debiased, trimmed and flat-field using a normalized flat field produced with apflatten. The spectra were extracted using doecslit with appropriate parameters. Wavelength calibration was performed by using the comparison spectrum of Thorium-Argon arcs. Flux calibration was accomplished through the observation of standard stars. The atmospheric extinction correction was also applied at the time of calibra-

tion using the mean extinction curve for La Palma. The seeing was less than 1.5 arc seconds.

Table 1 lists the global properties of our selected galaxies. Column 1 gives the galaxy name. Columns 2 and 3 give their coordinates. Columns 4-7 present their spectroscopic information from the literature: redshift, $H\beta$ flux, equivalent width of $H\beta$, and the Balmer decrement (Terlevich et al 1991, SCHG).

3. Data analysis

Figure 1 displays, for each galaxy, two panels. The larger left panel shows the direct image from DSS of a galaxy, while the right smaller panel (alongside the direct image) shows its Echelle CCD 2D spectrum. Superimposed on the direct image the location and position angle of the slit for our observation is indicated. In all cases the slit was centered on the brightest nucleus, as defined by broad band images. For those galaxies with a compact appearance the slit was aligned E-W, and for those which displayed a more extended structure, the slit was placed along the “extended” orientation. In the Echelle images, the horizontal direction represent the spatial dimension while the vertical is the dispersion direction. The image scales are given for both panels. The precise location in relation with the peak intensity is given in Table 2. Note that the spectrum of every subregion has been extracted using variable size apertures covering the extent of the $H\alpha$ emission. In all cases a large aperture including all the emission detected along the slit in each object has also been defined and subsequently referred to as the *total* emission.

The spectral range covered on each spectra includes $H\alpha$ ($\lambda 6563\text{\AA}$) and $[\text{NII}]\lambda\lambda 6583, 6548\text{\AA}$ lines. A clear $H\alpha$ emission is present on the spectra from all regions on all galaxies; The $[\text{NII}]$ doublet however only appears on some regions of three galaxies (Mrk59, IIZw70 and UM533). Thus, the analysis presented here is based on the behavior of the $H\alpha$ emission line of each galaxy.

There is a wide variety of spectral patterns. Some of them display a very well-behaved Gaussian $H\alpha$ line profile; others however, present clear signs of multiple spectral components. These, have been fitted using two (three in the case of IIZw70) Gaussian templates.

Table 2 lists the derived properties of the spectra of each of the recognized knots or regions as well as the *total* for each galaxy. Column 1 gives the galaxy name. Column 2 gives the *spatial* nomenclature. A clear peak in emission covered by the aperture is referred to as a “knot”, while “region” could represent a zone between knots or an extension. Total emission is the aperture covering all the emission arising from a galaxy. Column 3 gives the rotator position angle of the observation which corresponds to the slit position angle shown in Figure 1. Columns 4-5 provide the aperture position in relation to the main knot and size in arcsecs. Columns 6-8 refer to the analysis of the spectra and give the parameters obtained from Gaussian fits to the $H\alpha$ emission line, namely: $H\alpha$ flux, central wavelength and line width (FWHM in \AA). The typical error in flux are 10-20% estimated from the sensitivity curves from the standard star observations and ~ 5 -10% in line width from the comparison with the $H\beta$ line in the echelle observations or externally with different frames when available. In the cases where more than one Gaussian is needed to account for the $H\alpha$ emission line, the Table provides the various parameters derived for each of the components. The last column in Table 2 indicates the *spectral* nomenclature showing in some cases the presence of the additional spectral components from the emission line profile and their relative importance. A featureless emission line well fitted by a single Gaussian is referred as “single”, while “global” is a single fit to an emission line that shows more than one resolved component. This would mimic an observation with poorer spectral resolution. The main and secondary components of an emission line were also fitted whenever they arose.

The *global* (or *single*) Gaussian fit is a very good representation of the *total* $H\alpha$ line profile in spectrum of a galaxy, as shown in Figure 2. The results of the fit can be compared with parameters traditionally used to analyze the kinematics of H II regions by using single aperture spectroscopy (see Melnick *et al.* 1988 and Muñoz-Tuñón 1994 and references therein).

4. Results

Here we briefly describe the most general spectral features found in each galaxy of the sample.

TABLE 1
SPECTROSCOPIC DATA FROM TERLEVICH ETAL 1991, SCHG.

name	R.A. (1950)	δ (1950)	z	$-lgF(H\beta)$ [erg cm ² s ⁻¹]	$W(H\beta)$ [Å]	$C(H\beta)$
Mrk 59	12 56 38.2	35 06 53	0.0027	14.26	17	0.54
II Zw 70	14 48 55.2	35 46 36	0.0040			0.40
VIIZw403	11 24 35.8	79 16 03	-0.0003			0.40
Mrk 36	11 02 15.6	29 24 31	0.0022	13.36	70	0.44
UM 461	11 48 59.4	-2 05 41	0.0035	13.20	342	0.40
UM 533	12 57 25.0	2 19 08	0.0030	13.59	101	0.76
Mrk930	23 29 29.3	28 40 16	0.0181	13.05	71	0.55

FIGURE 1 = FIG1.JPG

Fig. 1.— Left larger panel: Direct image from DSS (North is up, East is left) with slit location indicated. Right smaller panel: Echelle CCD image on the H α spectral region (horizontal is the spatial direction, vertical is the dispersion direction).

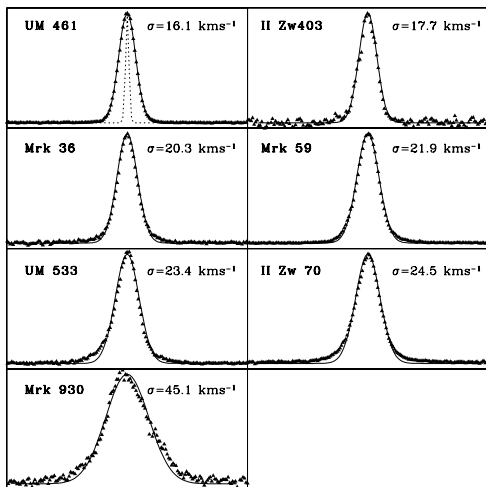


Fig. 2.— Emission line profiles of HII galaxies covering a range 10 Å centered on the H α line. Also shown are the Gaussian fits (solid lines) used to derive the final gas velocity widths which are given in the upper-right side of each panel and listed in Table 3. The comparison Thorium lamp line profile is shown in the first upper-left panel as a dotted line.

The qualitative description of each of these features is based on the precise measurements ie, the emission line parameters, given in Table 2.

From our results in Table 2 it is clear that even the apparently most compact of our H II galaxies (e.g. UM461; which spans across 11'') splits into several components, or emitting knots. Some of these may be true centers of stellar formation but others could simply be high density condensations ionized from the outside by the stellar radiation.

The emitting knots in every galaxy present different properties (intensity, line width, etc.) however in all cases the velocity dispersion extracted from the *total* fit to the spectra of every galaxy is, within the errors, identical to the velocity dispersion inferred for the main emitting knot found in every galaxy. This is a result now well established in the field of giant H II regions (e.g. Muñoz-Tuñón 1994, Sabalick *et al.* 1995, Muñoz-Tuñón *et al.* 1995). In the seven galaxies in our sample the main knot peak intensity amounts to half, or more, of the total intensity derived for the total fit. The other main components of other knots, in every galaxy, amount to less than an order of magnitude of the peak intensity of the total fit, and in many cases their line width is smaller than that derived for the main emitting knot. This is also the case for all secondary components required to fit low intensity line asymmetries, or shoulders, al-

TABLE 2
DERIVED SPECTRAL PROPERTIES.

name	KNOT ID	PA	Aperture [$^{\circ}$]		F(H α) [erg cm 2 s $^{-1}$]	Peak λ [\AA]	FWHM [\AA]	Spectral components
			pos.	size				
Mrk59	<i>total</i>	20		30.6	3.356E-13	6580.7	1.190	single
					9.270E-15	6601.4	1.170	single[NII]
	Main knot		0.0	10.6	3.710E-13	6580.7	1.173	single
	region 2		-17.6	6.2	3.270E-15	6581.1	0.870	single
	region 3		-8.2	5.2	1.730E-14	6581.2	1.347	<i>global</i>
					1.720E-14	6581.2	1.347	Main component
					2.860E-15	6579.8	0.800	Secondary component
	region 5		6.1	5.0	1.670E-14	6580.8	1.018	<i>global</i>
					1.590E-14	6580.8	0.960	Main component
				2.540E-15	6579.6	1.360	Secondary component	
II Zw70	<i>total</i>	45		19.9	2.686E-13	6589.2	1.320	single
					1.550E-14	6610.0	1.800	single[NII]
	Main knot		0.0	11.3	2.667E-13	6589.2	1.313	<i>global</i>
					1.680E-13	6589.2	0.850	Main component
					4.510E-14	6589.9	1.120	Secondary component
	region 2		10.18	8.6	6.000E-14	6588.4	1.020	Secondary component.
					5.374E-14	6589.2	1.423	<i>global</i>
					4.360E-14	6589.3	1.180	Main component
					4.060E-15	6590.5	1.480	Secondary component
				9.870E-15	6588.3	1.640	Secondary component	
	region 3		5.14	7.5	1.695E-14	6589.5	1.437	single
VI Zw403	<i>total</i>	45		18.4	5.650E-14	6560.7	0.980	single
	Main knot		0.0	9.7	2.754E-14	6560.7	0.986	single
	knot 2		7.8	3.7	8.938E-15	6560.6	0.829	single
	knot 3		11.1	3.7	4.560E-15	6560.5	1.048	<i>global</i>
					3.960E-15	6560.5	0.900	Main component
					4.290E-16	6559.6	0.610	Secondary component
	extension		20.7	23.9	7.968E-14	6560.7	1.013	poor S/N
Mrk36	<i>total</i>	90		15.1	1.650E-13	6577.4	1.108	<i>global</i>
					1.100E-13	6577.4	0.910	Main component
					5.840E-14	6577.4	1.870	low-intensity wings
	Main knot		0.0	8.1	1.115E-13	6577.4	1.036	<i>global</i>
					9.040E-14	6577.4	0.920	Main component
					2.640E-14	6577.4	2.270	low-intensity wings
	knot 2		4.3	4.0	4.721E-14	6577.5	1.336	single
	extension		7.9	5.0	1.129E-14	6577.6	1.373	<i>global</i>
UM461	<i>total</i>	90		11.4	2.085E-13	6586.1	0.906	single
	Main knot		0.0	6.1	1.938E-13	6586.1	0.905	single
	knot 2		5.6	4.4	1.449E-14	6586.8	0.870	single
UM533	<i>total</i>		90	14.8	1.309E-13	6582.8	1.263	<i>global</i>
					1.190E-13	6582.8	1.130	Main component
					1.350E-14	6581.6	1.180	low-intensity wings
					7.260E-15	6603.5	0.960	[NII]
	Main knot		0.0	7.4	1.146E-13	6582.7	1.258	single
					6.740E-15	6603.5	1.110	[NII]
	knot 2		-8.7	3.0	6.822E-15	6582.6	0.979	single
interknots		-4.5	4.4	5.927E-15	6582.3	0.789	single	
Mrk930	<i>total</i>	180		13.4	1.508E-13	6682.1	2.432	single
	Main knot		0.0	5.9	8.609E-14	6682.4	2.433	single
	knot 2		1.2	1.7	2.670E-14	6681.9	1.703	single
	knot 3		3.2	2.0	4.197E-14	6681.1	1.679	single
	knot 4		4.8	2.0	3.150E-14	6680.7	1.494	<i>global</i>
					2.316E-14	6680.5	1.160	Main component
				8.574E-15	6681.5	1.460	Secondary component	

though the peak intensity of these lines is usually much smaller. On the other hand, the secondary components required to fit the wing emission of some of the knots in every galaxy contribute by much less than an order of magnitude to the total emission and are in all cases very broad lines with line width values well above the value measured for the main emitting knot. Note however that uncertainties in the fit to low intensity wings are much larger.

Thus, the line emitting properties of H II galaxies, including their supersonic σ value are in all our cases dominated by the emitting properties of the most intense knot. And thus, similarly to giant H II regions, it seems that the main emitting knot reflects an intrinsic property generated by the recent starburst event (see Tenorio-Tagle *et al.* 1993, and Muñoz-Tuñón *et al.* 1996).

4.1. Notes on Individual Objects

4.1.1. Mrk 59

Mrk 59 has a NE-SW oriented "comet-like" optical appearance (see Figure 1). More recent studies have played special attention to this sub-class of H II galaxies (see Noeske *et al.* 2000). It shows a conspicuous bright region, which clearly dominates the emission, located at the tip of an extended tail. The optical nucleus contains a rich substructure in nebular emission. We have defined five sub-regions in total. A clear peak in luminosity (main knot) is however identified with a size (measured on the baseline of the $H\alpha$ line spatial profile) of ~ 10 arcseconds. At a much lower intensity level, there is an extended emission centered ~ 7 arcseconds from the main knot. In a similar way we have identified other intensity peaks showing emission along the slit which we named regions 2 and 3. In this galaxy the main knot intensity totally dominates the output of the emitting region.

4.1.2. II Zw 70

This is a very compact dwarf. Its image displays a single optical knot with some "disk-like" extended emission in broad band (see Figure 1). On the long slit Echelle CCD frame, one can see a clearly defined $H\alpha$ line as well as the [NII] doublet. The nebular emission spatial distribution is almost point-like with a slight asymmetry presenting an extended, lower intensity $H\alpha$ emission. The

nebular luminosity profile, led us to define three apertures from which we have extracted and analyzed the spectra. We refer to them as main knot (which overwhelmingly dominates the emission), region 2 and region 3. The $H\alpha$ emission line in the three apertures presents a remarkably symmetric profile, which however cannot be well fitted by a single Gaussian due to the presence of low-intensity wings. In fact a minimum of three Gaussians are needed to obtain a good fit. The values derived for the three components are given in Table 2.

4.1.3. VII Zw 403

This is a classical example of a very nearby blue compact galaxy. Its broad band optical morphology presents a typical core-halo structure with an extended light distribution. It has been the target of HST for studies of its stellar content (Schulte-Ladbeck *et al.* 1999a, 1999b). The distance to VII Zw 403 derived from these studies, and adopted here, is 4.4 Mpc.

From our data, we have identified along the slit a clear peak in emission: the main knot; which produces half of the luminosity of the galaxy. The spectrum of the main knot is well fitted by a single Gaussian with the possible presence of low intensity wings, too weak for being modeled. No signs of line splitting are seen at our present spectral resolution. Besides the main knot there are two additional intensity maxima (knots 2 and 3) very close to each other. The spectrum from knot 2 displays a Gaussian-like $H\alpha$ line. On knot 3 however, there seems to be a secondary component. The line can be reproduced by using two Gaussians, very close in wavelength (less than 1\AA). Moving along the slit, immediately behind the two secondary knots one finds an extended emission (named "extension" in Table 2), which despite the poor S/N we have fitted using a Gaussian, with parameters similar to those obtained from the fit to the *total* spectrum of the galaxy.

4.1.4. Mrk 36

Our echelle observations were taken with the slit oriented E-W (P.A. = 90) crossing the optical core of the galaxy. This object has been of particular interest because it shows a very "blobby" structure, most visible in near-IR images (Telles *et al.*

2000). However, our present observation crosses the bright nucleus which, as described below, also presents a well resolved structure. Bi-dimensional spectroscopy with Integral Field Units will be very valuable in the near future to unveil its internal kinematics and help us answer the question of the origin of the present starburst.

From the luminosity profile across the slit we have identified two main peaks of nebular emission (see Figure 1), labeled as main knot (the brightest one) and knot 2. Two more apertures have been defined for the analysis; *total* includes the whole emission from the galaxy and an extension which rescues the extended, low intensity emission besides knot 2.

The main knot, shows the dominant $H\alpha$ emission component. For the fitting to be successful also at the base of the line (low-intensity wings), a second Gaussian is needed. This has a much lower intensity but it is broader than the main component. The parameters obtained from doing the fitting with only one Gaussian are also presented on Table 2 and referred to as *global*. The secondary, low intensity, broad component is also present in the integrated (*total*) spectrum, which is clearly dominated by the emission from the brightest main knot.

4.1.5. *UM 461*

UM461 appears along the slit as a point-like source (see Figure 1). We extracted its spectra from an aperture covering the main knot. A secondary much weaker second peak, west from Main knot was also detected (knot 2). To compare the line profiles with those obtained using a single aperture spectrum, a third aperture covering all emission have been taken (*total*). The $H\alpha$ emission from the three apertures can be nicely fitted with a single Gaussian profile. The main knot dominates the total nebular emission of the galaxy and therefore the spectra from the main knot and the total are rather similar. It is important to notice that the second-weak knot (knot 2), although clearly spatially separated from the main one, shares its main kinematic parameters (see Table 2).

4.1.6. *UM 533*

Its optical appearance, as seen at the DSS is that of a halo which engulfs a heart-like core with

two clearly visible nuclei. Our slit was positioned in the E-W direction (P.A.=90) crossing the two nuclei. First thing to notice (see Figure 1) is that these two peaks are also visible in nebular emission. There the contrast is much larger, with a clear bright knot (Main knot) and a much weaker one, separated by about 10 arcsec (knot 2). To make a comparison and to find the spatial trend of the emission lines two more apertures were defined: an aperture covering the region in between knots 1 and 2 (interknots) and an aperture including the whole emitting region (*total*). In this galaxy [NII] (6583 Å) is also detected on the bright knot. The $H\alpha$ emission of the brightest knot shows a good Gaussian behavior on the line core, however at least a second Gaussian is needed to account for the emission arising from the line base. Low intensity wings are also evident on the spectra covering the whole emission, which, as mentioned before, is dominated by the brightest knot.

4.1.7. *Mrk 930*

This galaxy presents the largest redshift ($z = 0.018$) of our sample. It has a knotty appearance on the broad band image, and its nebular emission along the slit (located N-S, P.A.=180) also displays a multiple knot structure. The ensemble of knots seem to show at the same time a velocity trend (see Figure 1). From the luminosity profile four apertures, centered on each of the emission peaks (knots), were selected. The spectra from all of them are well reproduced with a single Gaussian profile, whose parameters are given in Table 2. The *total* spectrum, with a spatial beam of 14 arcseconds, covering all emission is also Gaussian-like, and presents the same σ value detected in the main knot. The main knot also accounts in this case for more than half of the total emission from the galaxy.

4.2. Structural parameters

Our echelle data has led us to built a comprehensive data base of sizes, velocity dispersion and luminosities of the galaxies of our sample; not only of the total parameters but also for the starbursts sub-structures found on each of them (Table 3).

Table 3 describes the derived physical parameters of our sample. Columns 1-2 identify the galaxy and the region or knot as described in Ta-

ble 2. Column 3 gives values of the velocity dispersion σ_{gas} obtained after correcting the observed line width (given in Table 2) for instrumental and thermal broadening ($\sigma_{gas}^2 = \sigma_{obs}^2 - \sigma_{inst}^2 - \sigma_{th}^2$), assuming a 10^4 K gas. Column 4 & 5 give the H α luminosity and the physical “radius” (Aperture size / 2) of a region or knot in pc. Column 6 gives an estimate of the H α surface brightness within the slit. Finally we give derived distances from their observed redshift z (except for VII Zw 403 as described above). Throughout this paper we use the current value of $H_0 = 65 \text{ km s}^{-1} \text{ Mpc}^{-1}$ (Suntzeff *et al.* 1999).

Our high quality data is here confronted to see if it is in agreement with previous statistical works which show that H II galaxies follow a luminosity *vs* σ ($L \propto \sigma^4$) and the size *vs* σ ($R \propto \sigma^2$) relationships. These correlations have often been obtained using single aperture spectroscopy and their validity under better spectral and spatial resolution is a key issue to be verified. Note that in each of our galaxies, the difference in the velocity centroids of the various components is in all cases less than 1 Å (from Table 2), and thus, the velocity shift between components cannot account on its own for the velocity dispersion detected in the total spectrum of a galaxy. The velocity dispersion in our data set thus reflects an intrinsic property of each of the components and in some cases this is indeed supersonic ($\sigma_{gas} > c_{HII}$; the sound speed in the ionized gas).

4.2.1. The $[L - \sigma]$ relation

Figure 3 plots our $L(\text{H}\alpha)$ *vs* σ for *all* the data from Table 3. The points were derived from single Gaussian fits to the spectral line of each aperture named *global* or *single* in the last column of Table 2. Measurements inferred from *total* apertures are shown as solid triangles. Open squares represent the values of the Main knot in each galaxy, while solid circles are other regions or secondary knots. In the plot, the size of the points is proportional to their H α surface brightness, (see Table 3).

Clearly the luminosity of the points representing the main knots (open squares) falls very close to values derived from apertures covering the *total* extent of the emitting region (solid triangles). The implication of this is that the brightest knot in every galaxy dominates almost entirely the total luminosity. In addition, the velocity dispersion

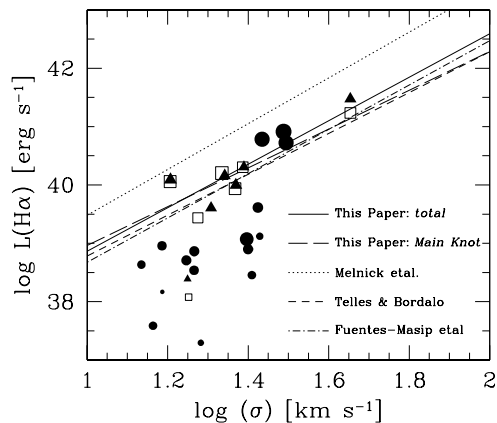


Fig. 3.— The luminosity - line width relation. Points: *total* apertures (solid triangles), Main Knot (open squares), other regions or knots (solid circles). Point sizes represent relative H α surface brightness. The lines are simple linear square fits for our data (total: solid line, Main knot: long dashes) and the statistical works from the literature.

TABLE 3

PHYSICAL PARAMETERS DERIVED FROM THE *single* GAUSSIAN FITS TO THE $H\alpha$ LINE (SEE TEXT FOR DETAILS). WE USE $H_0=65 \text{ km s}^{-1} \text{ Mpc}^{-1}$.

name	Knot ID	σ_{gas} [km s ⁻¹]	log(L(H α)) [erg s ⁻¹]	Radius [pc]	log SB [erg s ⁻¹ pc ⁻²]	Distance [Mpc]
Mrk 59	total	21.96	40.16	923	34.95	12.4
	Main knot	21.62	40.20	318	35.45	12.4
	knot 2	15.37	38.17	190	33.63	
	knot 3	25.11	38.90	163	34.43	
	knot 5	18.46	38.86	153	34.43	
II Zw 70	total	24.51	40.31	889	34.81	18.4
	Main knot	24.37	40.31	507	35.05	
	region2	26.56	39.61	387	34.47	
	region3	26.84	39.12	339	34.03	
VII Zw 403	total	17.76	38.39	196	34.30	4.4
	Main knot	17.88	38.08	104	34.26	
	knot2	14.58	37.59	39	34.19	
	knot3	19.16	37.30	39	33.90	
	extension	18.44	38.54	255	34.33	
Mrk 36	total	20.32	39.61	372	34.88	10.2
	Main knot	18.84	39.44	198	34.98	
	knot2	24.92	39.07	100	34.91	
	extension	25.66	38.46	126	34.19	
UM 461	total	16.10	40.09	450	35.07	16.2
	Main knot	16.08	40.06	238	35.32	
	knot2	15.34	38.96	177	34.33	
UM 533	total	23.41	40.00	498	35.00	13.9
	Main knot	23.31	39.94	248	35.25	
	knot2	17.64	38.71	101	34.41	
	interknot	13.64	38.64	144	34.19	
Mrk 930	total	45.06	41.48	2729	34.95	83.8
	Main knot	45.08	41.23	1197	35.07	
	knot2	31.21	40.72	341	35.10	
	knot3	30.76	40.91	407	35.22	
	knot4	27.21	40.79	405	35.10	

inferred for the main knots is almost identical to that derived from the total galactic emission.

A second thing to notice is the clear correlation displayed by either the total emitting spectra or by the main knots in our sample of galaxies (see Figure 2 and Table 4). This fit holds for all galaxies in our sample with the exception of VII Zw 403 which presents a $\log\sigma \sim 1.25$ and a $\log L(\text{H}\alpha) \sim 38$. Based on the work of Fuentes-Masip *et al.* (2000), where a thorough analysis of the luminosity and size *vs* velocity dispersion of the giant H II regions in the large irregular galaxy NGC 4449, led them to realize that the correlations only hold for nebulae with a supersonic line width and a surface brightness above $2 \times 10^{35} \text{ erg s}^{-1} \text{ pc}^{-2}$, we excluded this galaxy from our analysis. Note that VII Zw 403 is the galaxy with the lowest surface brightness in the sample. For this reason, we conclude that this object must fall below the threshold for which the relations hold (although the true luminosity threshold value cannot be established here). The surface brightness effect could be related to a second parameter in the relations, again similar to the fundamental plane of elliptical galaxies as Telles & Terlevich (1993) first attempted to investigate.

As far as the correlation is concerned (lines in Figure 3), we note that our present data either *total* (solid line) or *main knot* (long-dashed line) closely agree with the results from other works. Fuentes-Masip *et al.* (2000) results are shown as dot-dashed line. Telles & Bordalo (2000) analyzed a sample of about 40 H II galaxies and their preliminary results are shown as short-dashed lines. The similarity of these fits is evident in Figure 3. In the light of our results, we conclude that irrespectively of the structure that a galaxy (or a giant H II region) may have, the main emitting knot is likely to be sitting at the bottom of the gravitational potential well of its host galaxy, and therefore the overall motions are dominated by the mass of the complexes of gas and stars.

The existence of these relations and the presence of a surface brightness effect prompt us to suggest that the L *vs* σ relation may have an associated second parameter. This issue is being further investigated using 2D spectroscopy.

The numerical results of the various fits are shown in Table 4. Note however that the slope of the original Melnick *et al.* (1988) (L *vs* σ) relation

is virtually identical to all the others, although there is a clear offset on the zero point of their correlation, after all appropriate transformations are applied. This could be due to a systematic error in the calibration of their data, since independent calibration of Telles & Bordalo (2000) for a sample of a statistically significant sample of H II galaxies and the redshift independent zero points given by Fuentes-Masip *et al.* (2000) and Bosch (1999) for Giant H II Regions all agree within the uncertainties with the zero point measured here.

4.2.2. The $[R - \sigma]$ relation

Figure 4 shows the (R *vs* σ) relation for our present sample of H II galaxies. Again, measurements from *total* apertures are shown as solid triangles. Open squares represent the values for the main knots, while solid circles are other regions or knots. The sizes of the points are proportional to their corresponding $\text{H}\alpha$ surface brightness as given in Table 3.

From the analysis of this plot and the peak λ of all regions from Table 2 we conclude that no ordered motions are detected in these galaxies. The measured line widths are unlikely to be due to rotation, because as one goes down to smaller sizes (apertures) one still measures the same σ value (but see Van Zee *et al.*, 1998, who reach a different conclusion.)

As mentioned in many previous works about the topic, it is difficult to define a radial scale. Here we are considering the aperture size for each extraction of a spectrum which must be a scaled value to the true size of the emitting region. Even though, it is noticeable from Figure 4 that there is a clear correlation between size and the velocity dispersion for these objects, again, points with low surface brightness seem to fall out of the correlations. Also, there is a clear similarity between the slopes of the fit to the main knots (open squares, long-dashed line) and the total galaxy points (solid triangles, solid line). Both are very close to what one would expect for virialized systems. The results of the fits are given in Table 5. In addition, we note that these results (R_{total} and $R_{MainKnot}$ *vs* σ) are compatible with the findings of Telles (1995) for the size *vs* σ relation for H II galaxies, namely that the Effective Radius (derived from surface photometry) *vs* σ relation is a scaled version of the ‘‘Core’’ Radius (from luminosity pro-

TABLE 4

THE $[L - \sigma]$ SIMPLE LEAST SQUARE TO THE TOTAL APERTURE AND GLOBAL LINE FIT VALUES. ALSO SHOWN ARE THE RELATIONS FOUND FROM THE LITERATURE USING THE SAME SIMPLE LINEAR LEAST SQUARE FIT AND ALL TRANSFORMED TO $H_0=65 \text{ KM S}^{-1} \text{ MPC}^{-1}$ AS USED THROUGHOUT THIS PAPER.

	x	$L \propto x \times \log(\sigma)$ $\Xi \text{ [erg s}^{-1}\text{]}$	RMS
This paper	3.73 ± 1.01	35.14 ± 1.40	0.275
Melnick <i>et al.</i>	3.92 ± 0.47	35.55 ± 0.67	0.426
Telles & Bordalo	3.50 ± 0.67	35.28 ± 1.03	0.539
Fuentes-Masip <i>et al.</i>	3.80 ± 1.20	34.90 ± 1.70	

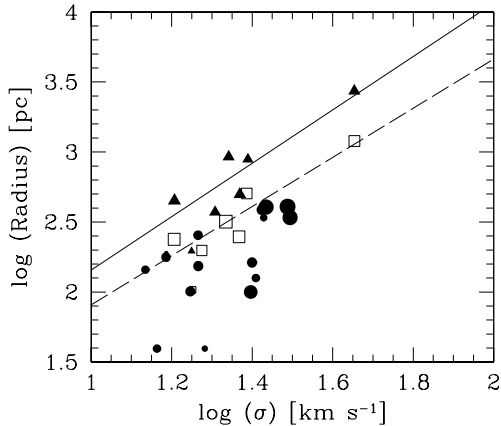


Fig. 4.— The Size - line width relation. Points: *total* apertures (solid triangles), Main Knot (open squares), other regions or knots (solid circles). Point sizes represent relative $H\alpha$ surface brightness. The lines are simple linear square fits for our data (total: solid line, Main knot: long dashes).

files) *vs* σ relation in a sample of about 40 galaxies, while the latter present a smaller scatter.

5. Discussion

Without a doubt, one of the most intricate issues in the field of giant H II regions, and now also of H II galaxies, is the origin of their supersonic velocity dispersion ($\sigma_{gas} > c_{HII}$).

It has long been established that a simple agglomeration of a large number of H II regions cannot lead to the dominant supersonic line profiles, and thus, giant H II regions, and H II galaxies, constitute a different class of objects. Different not only because of the size of their emitting regions and the fact that they are powered by recent violent bursts of star formation, but also because of their essence: their peculiar inner dynamics.

It is now well established that the supersonic line width correlates with the size of the emitting region (size $\propto \sigma^2$) and luminosity ($L \propto \sigma^4$) of the ionized regions (Terlevich & Melnick 1981, Melnick *et al.* 1987,1988, Telles & Terlevich 1993). The fact that the correlations are similar to the relations inherent to virialized stellar systems such as globular clusters, spiral bulges and the cores of elliptical galaxies, led Terlevich & Melnick to postulate that giant H II regions and H II galaxies are themselves virialized systems and thus that the measured gas velocity dispersion (σ_{gas}) should directly relate to their total mass. In their original scenario Terlevich & Melnick envisaged a gravitational potential that forced the collective motion of clumps of gas to present the supersonic σ values. However, in our sample and in the recent finding in giant H II regions the massive emitting

TABLE 5

THE $[R - \sigma]$ SIMPLE LEAST SQUARE TO THE TOTAL AND MAIN KNOT APERTURES VS. GLOBAL LINE FIT VALUES.

	y	$R \propto y \times \log(\sigma)$ Φ [pc]	RMS
<i>Total</i>	1.90±0.46	0.25±0.63	0.126
<i>Main Knot</i>	1.75±0.35	0.15±0.49	0.090

knots present a relative velocity unable to explain the observed supersonic σ values (see Tenorio-Tagle *et al.* 1993 1996, and references therein). Instead, the brightest knots present an intrinsic value of sigma formerly ascribed to the whole ionized region. This fine tuning regarding the size of the supersonic σ region and its luminosity has brought the empirical correlations into a much better agreement with what is expected from a virialized system. On the theory ground, virialization is now believed to have lots to do with the motion of the low-mass stars moving in the gravitational potential of the system while undergoing winds. This enhances their cross-section and allows them to cause the stirring of the gas left-over from the star formation event (see Tenorio-Tagle *et al.* 1993).

On the other hand, some authors have claimed that the supersonic line widths could result from a plethora of unresolved expanding shells caused by the mechanical energy of the large number of massive stars powering each of the sources (see Chu & Kennicutt 1994 and references therein). In the latter case however, there is no obvious way to explain the empirical correlations and thus it has been argued that the measured line widths follow the correlations simply due to a lack of resolution in the integrated spectra obtained from single aperture observations (but see also Tenorio-Tagle *et al.* 1996).

Our results confirm and extend the empirical correlations found for giant H II regions and H II galaxies. This fact has profound implications both on the observations of H II galaxies and on the interpretation of their supersonic line width. Enhanced spectral and spatial resolution seems to unveil an intricate structure in H II galaxies. Note that the previously measured (single aperture) su-

personic motions in fact arise from regions of much smaller dimension than that occupied by the full extent of the ionized gas. As shown in Figure 3 and Figure 4 for compact H II galaxies, accurate determinations of the size and luminosity of the region presenting the supersonic σ values nicely outline the correlations. H II galaxies when resolved, present several emitting knots with a variety of shapes, luminosity and σ values. However, we have shown that in these cases the global integrated value agree very closely with the properties derived for the main emitting knot. This is simply because the intrinsic properties (luminosity, velocity dispersion) of a galaxy are dominated by the central (core) component.

A fine calibration of these relations for local H II galaxies may be of great importance if used as a distance indicator of galaxies at large redshift, since H II galaxies are easy to find at great distances (see also Melnick *et al.* 2000). Particularly, as the global line emitting properties reflect the intrinsic properties of the central core component, observations even with poor spatial resolution could accurately define the luminosity and σ values of the dominant central core in every galaxy.

We thank Roberto Terlevich for a critical reading of the original version of this paper and for valuable discussion on this work. This study was partly financed by the Spanish DGES (Dirección General de Enseñanza Superior) (grant PB97-0158). GTT acknowledges partial support from Conacyt (México; grant 211290-5-28501E). GTT and CMT acknowledge the hospitality of the Observatório Nacional (Rio - Brasil) where part of this work was carried out. The WHT is operated on the island of La Palma by the ING at the Observatorio del Roque de los Muchachos. Finally,

we thank the anonymous referee for his/her comments that helped improve the presentation of our results.

REFERENCES

- Bosch, G., 1999, Ph.D. thesis, University of Cambridge
- Cairós, L.M., Vilchez, J.M., González-Pérez, J.N., Iglesias-Páramo, J. and Caon, N. 2000, ApJS, in press
- Chu, Y-H. & Kennicutt, R. 1994, ApJ 425, 720
- Doublier, V., Comte, G., Petrosian, A., Surace, C, Turatto, M., 1997, Astr. Astrophys. Suppl. , 124, 405
- Fuentes-Masip, O., Muñoz-Tuñón, C., Castañeda, H.O, & Tenorio-Tagle, G., 2000, AJ, 119, 2166
- Marlowe, A.T., Meurer, G.R. & Heckman, T.M., 1999, ApJ, 522, 183
- Melnick, J., 1979, ApJ, 228, 112
- Melnick, J., 1987, in “*Starburst and Galaxy Evolution*”, eds. T.X.Thuan, T.Montmerle & J.Tran Thanh Van, editions Frontières Gif Sur Yvette, France, p. 215
- Melnick, J., Moles M., Terlevich R. & Garcia-Pelayo J.M., 1987, MNRAS, 226, 849
- Melnick, J., Terlevich R. & Moles M., 1988, MNRAS, 235, 297
- Melnick, J., Terlevich, R. & Terlevich, E., 2000, MNRAS, 311, 629
- Muñoz-Tuñón, C., 1994, in Tenorio-Tagle, G. Ed., *Violent Star Formation: From 30 Doradus to QSOs*. Cambridge University Press. p 25
- Muñoz-Tuñón, C., Gavryusev, V. & Castañeda, H., 1995, AJ 110, 1630
- Muñoz-Tuñón, C., Tenorio-Tagle, G, Castañeda, H. & Terlevich, R., 1996, AJ 112, 1636
- Noeske, K.G., Guseva, N.G., Fricke, K.J., Izotov, Y.I., Papaderos, P. & Thuan, T.X., 2000, in “The Evolution of Galaxies. I- Observational Clues”, *Astrophys. Sp. Sc.* , in press
- Sabalisek, N., Tenorio-Tagle, G, Castañeda, H., Muñoz-Tuñón, C. 1995, ApJ 444, 200.
- Sargent W.L.W. & Searle L., 1970, ApJ, 162, L155
- Schulte-Ladbeck, R.E., Hopp, U., Greggio, L. & Crone, M.M., 1999a, AJ, 118, 2705
- Schulte-Ladbeck, R.E., Hopp, U., Crone, M.M. & Greggio, L., 1999b, ApJ, 525, 709
- Suntzeff, N.B., Phillips, M.M., Covarrubias, R., Navarrete, M., Peres, J.J.P., Guerra, A., Acevedo, M.T., Doyle, L.R., Harrison, T., Kane, S., Long, K.S., Maza, J., Miller, S., Pizzati, A.E., Claria, J.J., Ahumada, A.V., Pritzl, B., Winkler, P.F., 1999, AJ, 117, 1175
- Taylor, C.L 1997, ApJ, 480, 524
- Telles, E., 1995, Ph.D. thesis, University of Cambridge
- Telles, E. & Bordalo, V., 2000, in preparation
- Telles, E. & Maddox, S., 2000, MNRAS, 311, 307
- Telles, E. & Sampson, L., 2000, in “The Evolution of Galaxies. I- Observational Clues”, *Astrophys. Sp. Sc.* , in press
- Telles, E. & Terlevich, R., 1993, *Astrophys. Sp. Sc.* , 205, 49
- Telles, E. & Terlevich, R., 1995, MNRAS, 275, 1
- Telles, E. & Terlevich, R., 1997, MNRAS, 286, 183
- Telles, E., Melnick, J. & Terlevich, R., 1997, MNRAS, 288, 78
- Telles, E., Tapia, M., Terlevich, R., Kunth, D. & Sampson, L., 1999, in: K.A. van der Hucht, G. Koenigsberger & P.R.J. Eenens (eds.), “Wolf-Rayet Phenomena in Massive Stars and Starburst Galaxies”, *Proc. IAU Symposium No. 193* (San Francisco: ASP), 622
- Telles, E., Tapia, M., Terlevich, R., Kunth, D. & Sampson, L., 2000, in preparation
- Tenorio-Tagle, G., Muñoz-Tuñón, C. & Cox, D., 1993, ApJ 418, 767
- Tenorio-Tagle, G., Muñoz-Tuñón, C. & Cid-Fernandes, R., 1996, ApJ 456, 264

Terlevich, R. & Melnick, J., 1981, MNRAS, 195,
839

Terlevich, R., Melnick, J., Masegosa, J., Moles,
M. & Copetti, M.V.F., 1991, Astr. Astro-
phys. Suppl. , 91, 285 (SCHG)

Van Zee, L., Skillman, E.D. & Salzer, J.J., 1998,
ApJ, 116, 1186

This figure "fig1.jpg" is available in "jpg" format from:

<http://arxiv.org/ps/astro-ph/0010334v1>